Estimating Interception from Near-Surface Soil Moisture Response

Subodh Acharya[1*], Daniel McLaughlin[2], David Kaplan[3], and Matthew J. Cohen[1]

1 – School of Forest Resources and Conservation, University of Florida, Gainesville FL
2 – Department of Forest Resources and Conservation, Virginia Tech, Blacksburg, VA
3 – Environmental Engineering Sciences Department, University of Florida, Gainesville FL

* – Corresponding Author

Abstract

Interception is the storage and subsequent evaporation of rainfall by above-ground structures, including canopy and groundcover vegetation and surface litter. Accurately quantifying interception is critical for understanding how ecosystems partition incoming precipitation, but it is difficult and costly to measure, leading most studies to rely on modeled interception estimates. Moreover, forest interception estimates typically focus only on canopy storage, despite the potential for substantial interception by groundcover vegetation and surface litter. In this study, we developed an approach to quantify "total" interception (i.e., including forest canopy, understory, and surface litter layers) using measurements of shallow soil moisture dynamics during rainfall events. Across 34 pine and mixed forest stands in Florida (USA), we used soil moisture and precipitation (P) data to estimate interception storage capacity (β_s), a parameter required to estimate total annual interception (I_a) relative to P. Estimated values for β_s (mean β_s = 0.30 cm; $0.01 \leq \beta_s \leq 0.62$ cm) and I_a/P (mean $I_a/P = 0.14$; $0.06 \leq I_a/P \leq 0.21$) were broadly consistent with reported literature values for these ecosystems and were significantly predicted by forest structural attributes (leaf area index and percent groundcover), as well as other site variables (e.g., water table depth). The best-fit model was dominated by LAI and explained nearly 80% of observed β_s variation. These results suggest that whole-forest interception can be estimated using near-surface soil moisture time series, though additional direct comparisons would further support this assertion. Additionally, variability in interception across a single forest type underscores the need for expanded empirical measurement. Potential cost savings and logistical advantages of this method relative to conventional, labor-intensive interception measurements may improve empirical estimation of this critical water budget element.

Introduction

Rainfall interception (*I*) is the fraction of incident rainfall stored by above-ground ecosystem structures (i.e., vegetation and litter layers) and subsequently returned to the atmosphere via evaporation (*E*), never reaching the soil surface and thus never directly supporting transpiration (*T*) [*Savenije*, 2004]. Interception depends on climate and vegetation characteristics and can be as high as 50% of gross rainfall [*Gerrits et al.,* 2007; 2010; *Calder*, 1990]. Despite being critical for accurate water budget enumeration [*David et al*., 2006], interception is often disregarded or lumped with evapotranspiration (*ET*) in hydrological models [*Savenije*, 2004]. Recent work suggests interception uncertainty constrains efforts to partition *ET* into *T* and *E*, impairing representation of water use and yield in terrestrial ecosystems [*Wei et al.,* 2017].

When interception is explicitly considered, it is typically empirically estimated or modeled solely for the tree canopy. For example, direct measurements are often obtained from differences between total rainfall and water that passes through the canopy to elevated above-ground collectors (throughfall) plus water that runs down tree trunks (stemflow) during natural [e.g., *Bryant et al.,* 2005, *Ghimire et al.,* 2012, 2016] or simulated [e.g., *Guevara-Escobar et al.,* 2007; *Putuhena and Cordery,* 1996] rainfall events. This method yields the rainfall fraction held by and subsequently evaporated from the canopy but ignores interception by understory vegetation and litter. Alternatively, numerous empirical [e.g., *Merriam,* 1960], process-based [e.g., *Rutter et al.,* 1971, 1975; *Gash,* 1979, 1995, *Liu*, 1998], and stochastic [*Calder,* 1986] models are available for estimating interception. As with direct measurements, most model applications consider only canopy storage despite groundcover (both understory vegetation and litter layers) interception that can exceed canopy values in some settings [*Gerrits and Savenije*,

2011; *Putuhena and Cordery,* 1996]. As such, it seems likely that conventional measures and typical model applications underestimate actual (i.e., "total") interception.

New field approaches are needed to improve quantification of total interception and refine the calibration and application of available models. A detailed review of available interception models [*Muzylo et al.,* 2009] stresses the need for direct interception measurements across forest types and hydroclimatic regions, but meeting this need will require substantial methodological advances. Throughfall measurements yield direct and site-specific interception estimates [e.g., *Ghimire et al.,* 2017; *Bryant et al.,* 2005], but they are difficult and costly to implement even at the stand scale because of high spatial and temporal variability in vegetation structure [*Zimmerman et al.*, 2010; *Zimmerman and Zimmerman*, 2014]. Moreover, comprehensive measurements also require enumeration of spatially heterogeneous stemflow, as well as interception storage by the understory and litter layers, greatly exacerbating sampling complexity and cost [*Lundberg et al.,*1997]. Empirical techniques that estimate total interception, integrate across local spatial and temporal variation, and minimize field installation complexity are clearly desirable.

Here we present a novel approach for estimating total (i.e., canopy, understory and litter) interception using continuously logged, near-surface soil moisture. Prior to runoff generation, infiltration is equivalent to rainfall minus total interception, and the response of near-surface soil moisture during and directly following rain events can be used to inform interception parameters and thus interception. Since soil moisture is relatively easy and economical to measure continuously for extended periods, successful inference of interception from soil moisture time series may greatly expand the temporal and spatial domains of empirical interception measurements. As a proof-of-concept, we tested this simple interception estimation method in 34

93 forest plots spanning a wide range of conditions (e.g., tree density, composition, groundcover,
94 understory management, age, and hydrogeologic setting) across Florida (USA).
95
96 **Methods**
97 **Estimating Interception Storage Capacity from Soil Moisture Data**
98 During every rainfall event, a portion of the total precipitation (P) is temporarily stored in
99 the forest canopy and groundcover (hereafter referring to both live understory vegetation and
100 forest floor litter). We assume that infiltration (and thus any increase in soil moisture) begins
101 only after total interception storage, defined as the sum of canopy and groundcover storage, is
102 full. We further assume this stored water subsequently evaporates to meet atmospheric demand.
103 Calculating dynamic interception storage requires first determining the total storage capacity
104 (β_s), which is comprised of the storage capacities for the forest canopy (β_c) and groundcover (β_g)
105 (Fig. 1a).
106 To estimate β_s, we consider a population of individual rainfall events of varying depth
107 over a forest for which high frequency (i.e., 4 hr^{-1}) soil-moisture measurements are available
108 from near the soil surface. To ensure that canopy and groundcover layers are dry, and thus
109 interception storage is zero prior to rainfall onset (i.e., antecedent interception storage capacity =
110 β_s), we further filter the rainfall data to only include the events that are separated by at least 72
111 hours. Volumetric soil water content (θ) at the sensor changes only after rainfall fills β_s,
112 evaporative demands since rainfall onset are met, and there is sufficient infiltration for the
113 wetting-front to arrive at the sensor. Rainfall events large enough to induce a soil moisture
114 change ($\Delta\theta$) are evident as a rainfall threshold in the relationship between P and $\Delta\theta$. An example
115 time series of P and θ (Fig. 1b) yields a P versus $\Delta\theta$ relationship (Fig. 1c) with clear threshold

116 behavior. There are multiple equations whose functional forms allow for extraction of this
117 threshold; here we express this relationship as:

118 $$P = \frac{a}{\left(1+b*exp^{(-c*\Delta\theta)}\right)} \quad (1)$$

119 where P is the total rainfall event depth, $\Delta\theta$ is the corresponding soil moisture change, and a, b,
120 and c are fitted parameters. Figure 2 illustrates this relationship and model fitting for observed
121 $\Delta\theta$ data from six plots at one of our study sites described below. The y-intercept of Eq. 1 (i.e.,
122 where $\Delta\theta$ departs from zero) is given by:

123 $$P_s = \frac{a}{(1+b)} \quad (2)$$

124 where P_s represents the total rainfall required to saturate β_s, meet evaporative demands between
125 storm onset and observed $\Delta\theta$, and supply any infiltration required to induce soil moisture
126 response once β_s has been saturated. This equality can be expressed as:

127 $$P_s = \beta_s + \int_0^T E dt + \int_t^T f dt = \beta_s + \int_0^t E dt + \int_t^T E dt + \int_t^T f dt \quad (3)$$

128 where T is the total time from rainfall onset until observed change in θ (i.e., the wetting front
129 arrival), t is the time when β_s is satisfied, and E and f are the evaporation and infiltration rates,
130 respectively. To connect this empirical observation to existing analytical frameworks [.g., *Gash*
131 1979], we adopt the term P_G, defined as the rainfall depth needed to saturate β_s and supply
132 evaporative losses between rainfall onset (time = 0) and β_s saturation (time = t):

133 $$P_G = \beta_s + \int_0^t E dt \quad (4)$$

134 Solving for β_s in Eq. 3 and substituting into Eq. 4 yields:

135 $$P_G = P_s - \int_t^T E dt - \int_t^T f dt \quad (5)$$

136 Equation 5 may be simplified by assuming that average infiltration and evaporation rates apply
137 during the relatively short period between t and T, such that:

$$P_G = P_s - \bar{f}(T-t) - \bar{E}(T-t) \quad (6)$$

where $\bar{f}$ is the average soil infiltration rate and $\bar{E}$ is the average rate of evaporation from the forest surface (i.e., canopy, groundcover, and soil) during the time from t to T [see *Gash,* 1979]. The storage capacity β_s can now be calculated following Gash [1979] as:

$$\beta_s = -\frac{\bar{E}}{\bar{P}} \frac{P_G}{ln\left(1-\frac{\bar{E}}{\bar{P}}\right)} = -\frac{\bar{E}}{\bar{P}} \frac{[P_s-(T-t)(\bar{f}+\bar{E})]}{ln\left(1-\frac{\bar{E}}{\bar{P}}\right)} \quad (7)$$

where $\bar{P}$ is the average rainfall rate and all other variables are as previously defined. In Eq. 5, $\bar{E}$ is usually estimated using the Penman-Monteith equation [*Monteith,* 1965], setting canopy resistance to zero (e.g., *Ghimire et al.,* 2017).

A key challenge in applying Eq. 5, and thus for the overall approach, is quantifying infiltration, since the time, t, when β_s is satisfied is unknown. Moreover, the infiltration rate embedded in P_s is controlled by $\bar{P}$ and initial soil moisture content (θ_i). It is worth noting that shallower sensor depth placement would likely eliminate the need for this step (see Discussion). However, to overcome this limitation in our study (where our soil moisture sensor was 15 cm below the ground surface), we used the 1-D unsaturated flow model HYDRUS-1D [*Simunek et al.,* 1995] to simulate the required time for the wetting front to arrive (T_w) at the sensor under bare soil conditions across many combinations of $\bar{P}$ and θ_i. As such, T_w represents the time required for a soil moisture pulse to reach the sensor once infiltration begins (i.e., after β_s has been filled), which is T- t in Eq. 7. For each simulation, T_w (signaled by the first change in θ at sensor depth) was recorded and used to develop a statistical model of T_w as a function of $\bar{P}$and θ_i. We used plot-specific soil moisture retention parameters from Florida Soil Characterization Retrieval System (https://soils.ifas.ufl.edu/flsoils/) to develop these curves for our sites, but simulations can be applied for any soil with known or estimated parameters.

Simulations revealed that T_w at a specific depth declined exponentially with increasing θ_i:

$$T_w = ae^{-b\theta_i} \quad (8)$$

where a and b are fitting parameters. Moreover, the parameters a and b in Eq. (6) are well fitted by a power function of $\bar{P}$:

$$a = a_1\bar{P}^{a_2}, b = b_1\bar{P}^{b_2} \quad (9)$$

where a_1 and b_1 are fitting parameters. These relationships are illustrated in Fig. 3 for a loamy sand across a range of $\bar{P}$ and θ_i at 15 cm depth. The relationship between θ_i and T_w is very strong for small to moderate $\bar{P}$ (< 3.0 cm/hr). At higher values of $\bar{P}$, T_w is smaller than the 15-minute sampling resolution, and these events were excluded from our analysis (see below).

Assuming that $\bar{f}$ equals $\bar{P}$ over the initial infiltration period from t to T (robust for most soils, see below), Eq. 7 can be modified to:

$$\beta_s = \frac{-\bar{E}}{\bar{P}}\left[\frac{P_s - T_w(\bar{P}+\bar{E})}{ln\left(1-\frac{\bar{E}}{\bar{P}}\right)}\right] \quad (10)$$

This approach assumes no surface runoff or lateral soil-water flow near the top of the soil profile from time t to T. Except for very fine soils under extremely high $\bar{P}$, this assumption generally holds during early storm phases, before ponding occurs [*Mein and Larsen*, 1973]. However, where strong layering occurs near the surface, lateral flow above the sensor (i.e., at capillary barriers or differential conductivity layers; *Blume et al.,* 2009) may occur, and wetting front simulations described above would need to account for layered soil structure to avoid potential overestimation of interception. Lateral flow within the duff layer during high-intensity precipitation events as observed by Blume et al. (2008) would be more difficult to correct for, though we note that since our goal is to determine β_s, extreme storms can be omitted from the analysis when implementing Eqs. 1-10, without compromising β_s estimates. Similarly, not accounting for the presence of preferential flow (e.g., finger flow, funnel flow, or macropore

183 flow; *Orozco-Lopez et al.,* 2018) in wetting front calculations could lead to underestimation of
184 interception, though application in coarser texture soils (as evaluated here) likely minimize this
185 challenge. More generally, these limitations can be minimized by placing the soil moisture
186 sensor close to the soil surface (e.g., within 5 cm). Finally, we note that values of β_s from Eq. 10
187 represent combined interception from canopy and groundcover, but the method does not allow
188 for disaggregation of these two components.

189 **Calculating Interception**

190 Interception storage and subsequent evaporation (sometimes referred to as interception
191 loss) for a given rain event are driven by both antecedent rain (which fills storage) and
192 evaporation (which depletes it). Instantaneous available storage ranges from zero (saturated) to
193 the maximum capacity (i.e., β_s which occurs when the storage is empty). While discrete, event-
194 based interception models [*Gash,* 1979, 1995; *Liu*, 1998] have been widely applied to estimate
195 interception, continuous models more accurately represent time-varying dynamics in interception
196 storage and losses. We adopted the continuous, physically based interception modeling
197 framework of *Liu* [1998, 2001]:

198 $$I = \beta_s(D_0 - D) + \int_0^t (1 - D)Edt \quad (11)$$

199 where I is interception, D_0 is the forest dryness index at the beginning of the time step t, D is the
200 forest dryness index at time the end of t, and E is the evaporation rate from wetted surfaces. The
201 dryness index at each time-step is calculated as:

202 $$D = 1 - \frac{C}{\beta_s} \quad (12)$$

203 where C is "adherent storage" (i.e., water that does not drip to the ground) and is given by:

204 $$C = \beta_s \left(1 - D_0 exp\left(\frac{-(1-\tau)}{\beta_s} P\right)\right) \quad (13)$$

where τ is the free throughfall coefficient. Because our formulation of β_s in Eq. 10 incorporates both canopy and groundcover components (i.e., negligible true throughfall), we approximated τ in Eq. 13 as zero. Between rainfall events, water in interception storage evaporates to meet atmospheric demand, until the dryness index, D reaches unity [*Liu* 1997]. The rate of evaporation from wetted surfaces between rainfall events (E_s) is:

$$E_s = E(1 - D)exp\left(\frac{E}{\beta_s}\right) \quad (14)$$

A numerical version of Eq. 11 to calculate interception at each time step, *t*, is expressed as:

$$I = \beta_s(D_{t-1} - D_t) + \frac{1}{2}[E_{t-1}(1 - D_{t-1}) + E_t(1 - D_t)] \quad (15)$$

Eq. 15 quantifies continuous and cumulative interception using precipitation and other climate data (for E) along with β_s derived from soil moisture measurements and corresponding meteorological data.

Study Area and Data Collection

As part of a multi-year study quantifying forest water use under varying silvicultural management, we instrumented six sites across Florida, each with six 2-ha plots spanning a wide range of forest structural characteristics. Data from two of the plots at one site were not used here due to consistent surface water inundation, yielding a total of 34 experimental forest plots. Sites varied in hydroclimatic forcing (annual precipitation range: 131 to 154 cm/yr and potential *ET* range: 127 to 158 cm/yr) and hydrogeologic setting (shallow vs. deep groundwater table). Experimental plots within sites varied in tree species, age, density, leaf area index (LAI), groundcover vegetation density (%GC), soil type, and management history (Table 1). Each site contained a recent clear-cut plot, a mature pine plantation plot, and a restored longleaf pine (*Pinus palustris*) plot; the three remaining plots at each site included stands of slash pine (*Pinus elliottii*), sand pine (*Pinus clausa*), or loblolly pine (*Pinus taeda*) subjected to varying

228 silvicultural treatments (understory management, canopy thinning, prescribed burning) and
229 hardwood encroachment. The scope of the overall project (34 plots spanning 6 sites across
230 Florida) and the emphasis on measuring variation in forest ET and water yield precluded
231 conventional measurements of interception (e.g., throughfall and stemflow collectors). Because
232 model estimates of interception were considered sufficient for water yield predictions across
233 sites, the analyses presented here represent a proposal for additional insights about interception
234 that can be gleaned from time series of soil moisture rather than a meticulous comparison of
235 methods. We assessed results from this new method using comparisons with numerous previous
236 interception studies in pine stands in the southeastern US and elsewhere, and by testing for the
237 expected associations between estimated interception and stand structure (e.g., LAI and
238 groundcover).

239 Within each plot, three sets of TDR sensors (CS655, Campbell Scientific, Logan, UT,
240 USA) were installed to measure soil moisture at multiple soil depths (Fig. 1a). Only data from
241 the top-most sensor (15 cm below the ground surface) were used in this study. Soil-moisture
242 sensors were located to capture representative variation in stand geometry and structure (i.e.,
243 within and between tree rows) to capture variation in surface soil moisture response to rainfall
244 events. While this spatial layout was intended to characterize the range of plot-scale forest
245 canopy and groundcover heterogeneity, the three measurements locations were within a 10-m
246 radius and thus represent localized (sub-plot) interception estimates. Within each clear-cut plot at
247 each site, meteorological data (rainfall, air temperature, relative humidity, solar insolation, wind
248 speed and direction) were measured using a weather station (GRSW100, Campbell Scientific,
249 Logan, UT; Fig. 4c) every 3 seconds and used to calculate hourly E by setting the canopy
250 resistance to zero [*Ghimire et al.,* 2017; *Gash,* 1995; *Monteith,* 1965]. Growing season forest

canopy LAI (m^2 m^{-2}) and groundcover (%) were measured at every 5-m node within a 50 m x 50 m grid surrounding soil moisture measurement banks. LAI was measured at a height of 1 m using a LI-COR LAI-2200 plant canopy analyzer, and %GC was measured using a 1 m^2 quadrat.

To estimate β_s, mean $\Delta\theta$ values from the three surface sensors were calculated for all rainfall events separated by at least 72 hours. Storm separation was necessary to ensure the canopy and groundcover surfaces were mostly dry (and thus antecedent storage capacity = β_s) at the onset of each included rainfall event. Rainfall events were binned into discrete classes by depth and plotted against mean $\Delta\theta$ to empirically estimate P_s (e.g., Fig. 2). For each rainfall bin, mean θ_i, $\bar{P}$ and $\bar{E}$ were also calculated to use in Eq. 10, which was then applied to calculate β_s. Subsequently, we developed generalized linear models (GLMs) using forest canopy structure (site-mean LAI), mean groundcover (% GC), hydrogeologic setting (shallow vs. deep groundwater table), and site as potential predictors, along with their interactions, to statistically assess predictors of β_s estimates. Because models differed in fitted parameter number, the best model was selected using the Akaike Information Criteria (AIC; *Akaike,* 1974). Finally, we calculated cumulative annual interception (I_a) and its proportion of total precipitation (I_a/P) for each study plot using the mean β_s for each plot (across the 3 sensor banks), climate data from 2014 to 2016, and Eq. 15. Differences in I_a/P across sites and among plots within sites were assessed using ANOVAs. All analyses were performed using R [*R Core Team,* 2017].

Results

Total Storage Capacity (β_s)

The exponential function used to describe the P-$\Delta\theta$ relationship (Eq. 1) showed strong agreement with observations at all sites and plots (overall $R^2 = 0.80$; $0.47 \leq R^2 \leq 0.97$; Table 1)

as illustrated for a single site in Fig. 2. This consistency across plots and sites suggests that Eq. 1 is capable of adequately describing observed P-$\Delta\theta$ relationships, enabling estimates of β_s across diverse hydroclimatic settings and forest structural variation. Estimates of β_s ranged from 0.01 to 0.62 cm, with a mean of 0.30 cm (Table 1). Plot-scale LAI was moderately correlated with plot-mean β_s, describing roughly 32% of observed variation across plots (Fig. 4a). This relatively weak association may arise because LAI measurements only characterize canopy cover, while β_s combines canopy and groundcover storage. The best GLM of β_s (Fig. 4b) used %GC and an interaction term between site and LAI ($R^2 = 0.84$ and AIC = 253.7, Table 2). The best GLM without site used LAI and hydrogeologic setting (shallow vs. deep water table) but had reduced performance ($R^2 = 0.55$ and AIC = 338.3; Table 2). All models excluding LAI as a predictor performed poorly, so we report model comparisons only for those including LAI.

Annual Interception (I_a)

Despite having similar rainfall regimes (mean annual precipitation ranging from 131 to 154 cm yr^{-1} across sites), mean annual interception (I_a) differed significantly both across sites (one-way ANOVA $p < 0.001$) and among plots within sites (one-way ANOVA $p < 0.001$). Estimates of I_a/P across all plots and sites ranged from 6 to 21% of annual rainfall (Table 1) and were moderately, but significantly, correlated with mean LAI, explaining approximately 30% of variation in I_a/P (Fig. 5a). Correlations among I_a/P and LAI were stronger for individual sites than the global relationship ($0.51 \leq R^2 \leq 0.84$), except for site EF, where I_a was small and similar across plots regardless of LAI (Fig. 5b; Table 1). This suggests that additional site-level differences (e.g., hydroclimate, soils, geology) play a role in driving I_a, as expected following from their effects on β_s described above.

Discussion

When combined with local rainfall data, near-surface soil moisture dynamics inherently contain information about rainfall interception by above-ground structures. Using soil moisture data, we developed and tested an analytical approach for estimating total interception storage capacity (β_s) that includes canopy, understory, and groundcover vegetation, as well as any litter on the forest floor. The range of β_s given by our analysis (mean β_s = 0.30 cm; $0.01 \leq \beta_s \leq 0.62$ cm) is close to, but generally higher than previously reported canopy-only storage capacity values for similar pine forests (e.g., 0.17 to 0.20 cm for mature southeastern USA pine forests; *Bryant et al*. 2005). Moreover, our estimates of β_s and annual interception corresponded to expected forest structure controls (e.g., LAI and ground cover) on interception, further supporting the feasibility of the soil moisture-based approach. However, we emphasize that a more robust validation of the method using co-located and contemporaneous measurement using standard techniques is warranted. Below we summarize the assumptions and methodological considerations that affect the potential utility and limitation of the method.

An important distinction between our method and previous interception measurement approaches is that the soil moisture-based method estimates composite rainfall interception of not only the canopy, but also of the groundcover vegetation and forest floor litter. Rainfall storage and subsequent evaporation from groundcover vegetation and litter layers can be as high, or higher than, canopy storage in many forest landscapes [*Putuhena and Cordery,* 1996; *Gerrits et al.,* 2010]. For example, *Li et al.* [2017] found that the storage capacity of a pine forest floor in China was between 0.3 and 0.5 cm, while maximum canopy storage was < 0.1 cm. *Putuhena and Cordery* [1996] also estimated storage capacity of pine forest litter to be approximately 0.3 cm based on direct field measurements. *Gerrits et al.* [2007] found forest floor interception to be

34% of measured precipitation in a beech forest, while other studies have shown that interception by litter can range from 8 to 18% of total rainfall [*Gerrits et al.,* 2010; *Tsiko et al.,* 2012; *Miller et al.,* 1990; *Pathak et al.,* 1985; *Kelliher et al.,* 1992]. A recent study using leaf wetness observations [*Acharya et al.,* 2017] found the storage capacity of eastern redcedar (*Juniperus virginiana*) forest litter to range from 0.12 to as high as 1.12 cm, with forest litter intercepting approximately 8% of gross rainfall over a six-month period. Given the composite nature of forest interception storage and the range of storage capacities reported in these studies, the values we report appear to be plausible and consistent with the expected differences between canopy-only and total interception storage.

Interception varies spatially and temporally and is driven by both β_s and climatic variation (i.e., P and E). Our approach represents storage dynamics by combining empirically derived β_s estimates with climatic data using a previously developed continuous interception model [*Liu* 1998, 2001]. Cumulative I_a estimates in this study ranged considerably (i.e., from 6% to 21% of annual rainfall) across the 34 plots, which were characterized by variation in canopy structure ($0.12 < \text{LAI} < 3.70$) and groundcover ($7.9 < \%\text{GC} < 86.2$). In comparison, interception by pine forests reported in the literature (all of which report either canopy-only or groundcover-only values, but not their composite) range from 12 to 49% of incoming rainfall [*Bryant et al.,* 2005; *Llorens et al.,* 1997; *Kelliher and Whitehead,* 1992; *Crockford and Richardson,* 1990]. Notably, most of the variation in this range is driven by climate rather than forest structure, with the highest I_a values from more arid regions [e.g., Llorens et al. 1997]. Future work could also consider seasonally disaggregated measurements to explore intra-annual variation in canopy structure and litter composition [Van Stan et al. 2017].

341 Broad agreement between our results and literature I_a values again supports the potential
342 utility of our method for estimating this difficult-to-measure component of the water budget,
343 though additional direct comparisons would further support this assertion. Additionally, the
344 magnitude and heterogeneity of our I_a estimates across a single forest type (southeastern US
345 pine) underscores the urgent need for empirical measurements of interception that incorporate
346 information on both canopy and groundcover storage in order to develop accurate water budgets.
347 This conclusion is further bolstered by the persistent importance of site-level statistical effects in
348 predicting β_s (and therefore I_a), even after accounting for forest structural attributes, which
349 suggests there are influential edaphic or structural attributes that we are not currently adequately
350 assessing. For example, while estimated I_a in clear-cut plots was generally smaller than plots
351 with a developed canopy, as expected, one exception was at EF where the clear-cut plot
352 exhibited the highest I_a of the six EF plots (8.4%, Table 1). However, differences among all EF
353 plots were very small (I_a ranged only from 7.9 to 8.4 % of annual rainfall), a rate consistent with
354 or even lower than other clear cuts across the study. This site is extremely well drained with
355 nutrient-poor sandy soils and differs from other sites in that it has dense litter dominated by
356 mosses, highlighting the need for additional local measurements to better understand how forest
357 structure controls observed interception.
358 There are several important methodological considerations and assumptions inherent to
359 estimating interception using near-surface soil moisture data. First is the depth at which soil
360 moisture is measured. Ideally, θ would be measured a few centimeters into the soil profile,
361 eliminating the need to account for infiltration when calculating P_G in Eqs. (4-6) and thereby
362 alleviating concerns about lateral and preferential flow. Soil moisture data used here were
363 leveraged from a study of forest water yield, with sensor deployment depths selected to

364 efficiently integrate soil moisture patterns through the vadose zone. The extra step of modeling
365 infiltration likely increases uncertainty in β_s given field-scale heterogeneity in soil properties and
366 potential lateral and preferential flow. Specifically, lateral flow would delay wetting-front
367 arrival, leading to overestimation of interception, while preferential flow would do the opposite.
368 Despite these caveats, infiltration in our system was extremely well-described using wetting
369 front simulations of arrival time based on initial soil moisture and rainfall. As such, while we
370 advocate for shallower sensor installation and direct comparison to standard methods in future
371 efforts, the results presented here given the available sensor depth seem tenable for this and other
372 similar data sets.

373 Another methodological consideration is that, in contrast to the original Gash (1979)
374 formulation, Eq. 5 does not explicitly include throughfall. While throughfall has been a critical
375 consideration for rainfall partitioning by the forest canopy, our approach considers total
376 interception by aboveground forest structures (canopy, groundcover, and litter). A portion of
377 canopy throughfall is captured by non-canopy storage and thus intercepted. Constraining this
378 fraction is not possible with the data available, and indeed our soil moisture response reflects the
379 "throughfall" passing the canopy, understory and litter. Similarly, estimation of β_s using Eqs. 1-7
380 cannot directly account for stemflow, which can be an important component of rainfall
381 partitioning in forests [e.g., *Bryant et al.,* 2005]. We used the mean soil moisture response across
382 three sensor locations (close to a tree, away from the tree but below the canopy, and within inter-
383 canopy rows), which lessens the impact of this assumption on our estimates of β_s. Finally, Eqs.
384 (3-10) assume the same evaporation rate, E, for intercepted water from the canopy and from the
385 understory. Evaporation rates may vary substantially between the canopy, understory, and forest
386 floor [*Gerrits et al.,* 2007, 2010], especially in more energy-limited environments. Future work

should consider differential evaporation rates within each interception storage, particularly since the inclusion of litter as a component potentially accentuates these contrasts in *E*.

Among the many challenges of measuring interception is the spatial heterogeneity of canopy and ground cover layers, with associated heterogeneity in interception rates. Consequently, researchers have suggested that 25 funnel collectors per hectare (or more) are necessary to maintain mean relative error below 10% for long-term monitoring, with as many as 200 collectors needed for similar error rates during event sampling [*Zimmerman et al.,* 2010; *Zimmerman and Zimmerman,* 2014]. Spatial averaging using larger trough collectors obviates some of this sampling effort, yielding guidance of 5 trough collectors per hectare [*Zimmerman and Zimmerman,* 2014], but still misses stemflow and groundcover variation. While the spatial integration extent of troughs versus soil moisture sensors remains unknown, the three soil moisture sensors we deployed per plot (with sensor locations selected to span stand spatial heterogeneity) seem likely to capture similar spatial extents. Moreover, the strong correspondence between our measurements and literature reported values for the magnitude of interception storage as well as the forest structure controls (i.e., LAI and ground cover) on that storage volume underscores that soil moisture measurements, at least in this setting, integrate key quantitative aspects of the interception process.

If soil moisture measurements were subject to the same fine-grained spatial heterogeneity as funnel-type collectors, it seems highly unlikely that our results would comport with literature expectations as closely as they do. One plausible explanation for the consistency of our results is that soil moisture averages across extant spatial heterogeneity in canopy processes, allowing soil moisture measurements to provide comparable spatial integration to throughfall troughs, without the considerable maintenance of litter accumulation associated with those troughs. This finding

410 is concordant with results from Metzger et al. (2017), who found correspondence between
411 throughfall and soil moisture changes across storm events of different sizes, leading these
412 authors to conclude that "net precipitation" can be intuited using soil water dynamics. Additional
413 soil moisture measurements would undoubtedly improve the accuracy of field estimates, and
414 indeed we recommend that more direct methodological comparisons are needed. However, our
415 results support the general applicability of the soil moisture-based approach for developing forest
416 interception estimates across a wide range of hydroclimatic and forest structural settings.
417

418 **Conclusions**

419 Rainfall interception by forests is a dynamic process that is strongly influenced by
420 rainfall patterns (e.g., frequency, intensity), along with various forest structural attributes such as
421 interception storage capacity (β_s) [*Gerrits et al.,* 2010]. In this work, we coupled estimation of a
422 total (or "whole-forest") β_s parameter with a continuous water balance model [*Liu,* 1997, 2001;
423 *Rutter et al.,* 1975], providing an integrative approach for quantifying time-varying and
424 cumulative interception. We propose that soil moisture-based estimates of β_s have the potential
425 to more easily and appropriately represent combined forest interception relative to existing time-
426 and labor-intensive field methods that fail to account for groundcover and litter interception.
427 However, we emphasize that further experimental work is needed to validate this promising
428 approach. Soil moisture can be measured relatively inexpensively and easily using continuous
429 logging sensors that require little field maintenance, facilitating application of the presented
430 approach across large spatial and temporal extents and reducing the time and resources that are
431 needed for other empirical measures [e.g., *Lundberg et al.,* 1997]. Finally, while our comparisons
432 with other empirical measures of forest canopy interception should be treated cautiously, this

433 approach yields values that are broadly consistent with the literature, and provide an estimate of
434 combined canopy and groundcover storage capacity that has the potential to improve the
435 accuracy of water balances models at scales from the soil column to watershed.
436
437 **References**

438 Acharya, B.S., Stebler, E., and Zou, C.B.: Monitoring litter interception of rainfall using leaf
439 wetness sensor under controlled and field conditions. *Hydrological Processes,* 31, 240-
440 249: DOI: 10.1002/hyp.11047, 2005

441 Benyon, R.G., Doody, and T. M.: Comparison of interception, forest floor evaporation and
442 transpiration in *Pinus radiata* and *Eucalyptus globulus* plantations. *Hydrological*
443 *Processes* **29** (6): 1173–1187 DOI: 10.1002/hyp.10237, 2015

444 Blume, T., Zehe, E. and Bronstert, A.: Use of soil moisture dynamics and patterns at different
445 spatio-temporal scales for the investigation of subsurface flow processes. *Hydrology and*
446 *Earth System Sciences*, **13(7)**: 1215-1233, 2009

447 Blume, T., Zehe, E., and Bronstert, A. : Investigation of runoff generation in a pristine, poorly
448 gauged catchment in the Chilean An- des. II: Qualitative and quantitative use of tracers
449 at three differ- ent spatial scales. Hydrol. Proc., **22**: 3676–3688, 2008

450 Bryant, M.L., Bhat, S., and Jacobs, J.M.: Measurements and modeling of throughfall variability
451 for five forest communities in the southeastern US. *Journal of Hydrology*, DOI:
452 10.1016/j.jhydrol.2005.02.012, 2005

453 Bulcock, H.H., and Jewitt, G.P.W.: Modelling canopy and litter interception in commercial
454 forest plantations in South Africa using the Variable Storage Gash model and idealized
455 drying curves. *Hydrol. Earth Syst. Sci* **16**: 4693–4705 DOI: 10.5194/hess-16-4693-2012,
456 2012

457 Calder, I. R.: A stochastic model of rainfall interception. *Journal of Hydrology*, **89**: 65-71, doi:
458 10.1016/0022-1694(86)90143-5, 1986

459 Calder, I.R.: Evaporation in the Uplands. Wiley, New York, pp. 148, 1990

460 Carlyle-Moses, D.E., and Gash, J.H.C.: Rainfall Interception Loss by Forest Canopies. *In*
461 Carlyle-Moses and Tanaka (Eds), *Ecological Studies* 216. DOI: 10.1007/978-94-007-
462 1363, 2011

463 Carlyle-Moses, D.E., and Price, A.G.: Modelling canopy interception loss from a Mediterranean
464 pine-oak stand, northeastern Mexico. *Hydrological Processes* **21** (19): 2572–2580 DOI:
465 10.1002/hyp.6790, 2007

Crockford, R.H., and Richardson, D.P.: Partitioning of rainfall into throughfall, stemflow and interception: effect of forest type, ground cover and climate. *Hydrological Processes* **14** (16–17): 2903–2920 DOI: 10.1002/1099-1085(200011/12)14:16/17<2903::AID-HYP126>3.0.CO;2-6, 2000

David, T. S., Gash, J.H. C., Valente, F., Pereira, J. S., Ferreira, M.I. and David, J. S.: Rainfall interception by an isolated evergreen oak tree in aMediterranean savannah.*Hydrological Processes* **20**: 2713–2726. DOI: 10.1002/hyp.6062, 2006

Gash, J.H.C., Lloyd, C.R., and Lachaud, B. G.: Estimating sparse forest rainfall interception with an analytical model. *Journal of Hydrology* **170**: 79–86, 1995

Gash, J.H.C.: An analytical model of rainfall interception by forests. *Quarterly Journal of the Royal Meteorological Society* **105** (443): 43–55 DOI: 10.1002/qj.49710544304, 1979

Gerrits, A.M.J., Savenije, H.H.G., Hofmann, L., and Pfister, L.: New technique to measure forest floor interception – an application in a beech forest in Luxembourg. *Hydrol. Earth Syst. Sci* **11**: 695–701, 2007

Ghimire, C.P., Bruijnzeel, L.A., Lubczynski, M.W., and Bonell, M.: Rainfall interception by natural and planted forests in the Middle Mountains of Central Nepal. *Journal of Hydrology* **475**: 270–280 DOI: 10.1016/j.jhydrol.2012.09.051, 2012

Ghimire, C.P., Bruijnzell, L.A., Lubczynski, M.W., Ravelona, M., Zwartendijk, B.W., and Meervald, H.H.: Measurement and modeling of rainfall interception by two differently aged secondary forests in upland eastern Madagascar, Journal of Hydrology, DOI: 10.1016/j.jhydrol.2016.10.032, 2017

Jarvis, N.J., Moeys, J. Koestel, J., and J.M. Hollis.: Preferential flow in a pedological perspective. In: Lin, H. , editor, Hydropedology: Synergistic integration of soil science and hydrology. Academic Press, Waltham, MA. p. 75–120. doi:10.1016/B978-0-12-386941-8.00003-4, 2012.: Understanding preferential flow in the vadose zone: Recent advances and future prospects. Vadose Zone J. **15 (12)**. doi:10.2136/vzj2016.09.0075, 2016

Kelliher, F.M., Whitehead, D., and Pollock D.S.: Rainfall interception by trees and slash in a young Pinus radiata D. Don stand. *Journal of Hydrology* **131** (1–4): 187–204 DOI: 10.1016/0022-1694(92)90217-J, 1992

Li, X., Xiao, Q., Niu, J., Dymond, S., Mcherson, E. G., van Doorn, N., Yu, X., Xie, B., Zhang, K., and Li, J.: Rainfall interception by tree crown and leaf litter: an interactive process. *Hydrological Processes* DOI: 10.1002/hyp.11275, 2017

Liu, J.: A theoretical model of the process of rainfall interception in forest canopy. *Ecological Modelling* **42**: 111–123, 1988

Liu, S.: A new model for the prediction of rainfall interception in forest canopies. *Ecological Modelling* **99**: 15–159, 2001

Liu, S.: Estimation of rainfall storage capacity in the canopies of cypress wetlands and slash pine uplands in North-Central Florida. *Journal of Hydrology* **207**: 32–41, 1998

Liu, S.: Evaluation of the Liu model for predicting rainfall interception in forests world-wide. *Hydrological Processes* **15** (12): 2341–2360 DOI: 10.1002/hyp.264, 2001

Llorens, P., and Poch, R.: Rainfall interception by a *Pinus sylvestris* forest patch overgrown in a Mediterranean mountainous abandoned area I. Monitoring design and results down to the event scale. *Journal of Hydrology* **199**: 331–345, 1997

Lundberg, A., Eriksson, M., Halldin, S., Kellner, E., and Seibert, J.: New approach to the measurement of interception evaporation. Journal of Atmospheric and Oceanic Technology 14 (5), 1023–1035, 1997

Massman, W.J.: The derivation and validation of a new model for the interception of rainfall by forests. *Agricultural and Forest Meteorology* **28**: 261–286, 1983

Merriam, R.A.: A note on the interception loss equation. *Journal of Geophysical Research* **65** (11): 3850–3851 DOI 10.1029/JZ065i011p03850, 1960

Metzger, J.C., Wutzler, T., Dalla Valle, N., Filipzik, J., Grauer, C., Lehmann, R., Roggenbuck, M., Schelhorn, D., Weckmüller, J., Küsel, K. and Totsche, K.U., 2017. Vegetation impacts soil water content patterns by shaping canopy water fluxes and soil properties. *Hydrological processes*, *31*(22), pp.3783-3795.

Muzylo, A., Llorens, P., Valente, F., Keizer, J.J., Domingo, F., and Gash, J.H.C. Gash. A review of rainfall interception modelling. *Journal of Hydrology* **370**: 191–206 DOI: 10.1016/j.jhydrol.2009.02.058, 2009

Orozco-López, E., Muñoz-Carpena, R., Gao, B., and Fox, G.A.: Riparian vadose zone preferential flow: Review of concepts, limitations, and perspectives. Vadose Zone Journal **17**: doi: 10.2136/vzj2018.02.0031, 2018

Pook, E.W., Moore, P.H.R., and Hall, T.: Rainfall interception by trees of *Pinus radiata* and *Eucalyptus viminali* in a 1300 mm rainfall area of southeastern New South Wales: I. Gross losses and their variability. *Hydrological Processes* **5** (2): 127–141 DOI: 10.1002/hyp.3360050202, 1991

Putuhena, W.M., and Cordery, I.: Estimation of interception capacity of the forest floor. *Journal of Hydrology* **180**: 283–299, 1996

Rutter, A.J., Morton, A.J., and Robins, P.C.: A Predictive Model of Rainfall Interception in Forests. II. Generalization of the Model and Comparison with Observations in Some Coniferous and Hardwood Stands *Journal of Applied Ecology* **12** (1): 367–380, 1975

Savenije, H. H. G.: The importance of interception and why we should delete the term evapotranspiration from our vocabulary, Hydrol. Processes, 18, 1507 – 1511, 2004

Schaap, M.G., Bouten, W., and Verstraten, J.M.: Forest floor water content dynamics in a Douglas fir stand. *Journal of Hydrology* **201**: 367–383, 1997

Valente, F., David, J.S., and Gash, J.H.C.: Modelling interception loss for two sparse eucalypt and pine forests in central Portugal using reformulated Rutter and Gash analytical models. *Journal of Hydrology* **190**: 141–162, 1997

Van Dijk, A.I.J.M., and Bruijnzeel, L.A.: Modelling rainfall interception by vegetation of variable density using an adapted analytical model. Part 1. Model description. Journal of Hydrology, 247:230-238, 2001

Wei, Z., Yoshimura, K., Wang, L., Miralles, D.G., Jasechko, S., and Lee, X.: Revisiting the contribution of transpiration to global terrestrial evapotranspiration. *Geophysical Research Letters* **44** (6): 2792–2801 DOI: 10.1002/2016GL072235, 2017

Xiao, Q., McPherson, E.G., Ustin, S.L., and Grismer, M.E.: A new approach to modeling tree rainfall interception. *Journal of Geophysical Research: Atmospheres* **105** (D23): 29173–29188 DOI: 10.1029/2000JD900343, 2000

Zimmermann, A. and Zimmermann, B.: Requirements for throughfall monitoring: The roles of temporal scale and canopy complexity. Agricultural and forest meteorology, **189**, 125-139, 2014

Zimmermann, B., Zimmermann, A., Lark, R.M. and Elsenbeer, H.: Sampling procedures for throughfall monitoring: a simulation study. Water Resources Research, **46(1)**: doi: 10.1029/2009WR007776, 2010

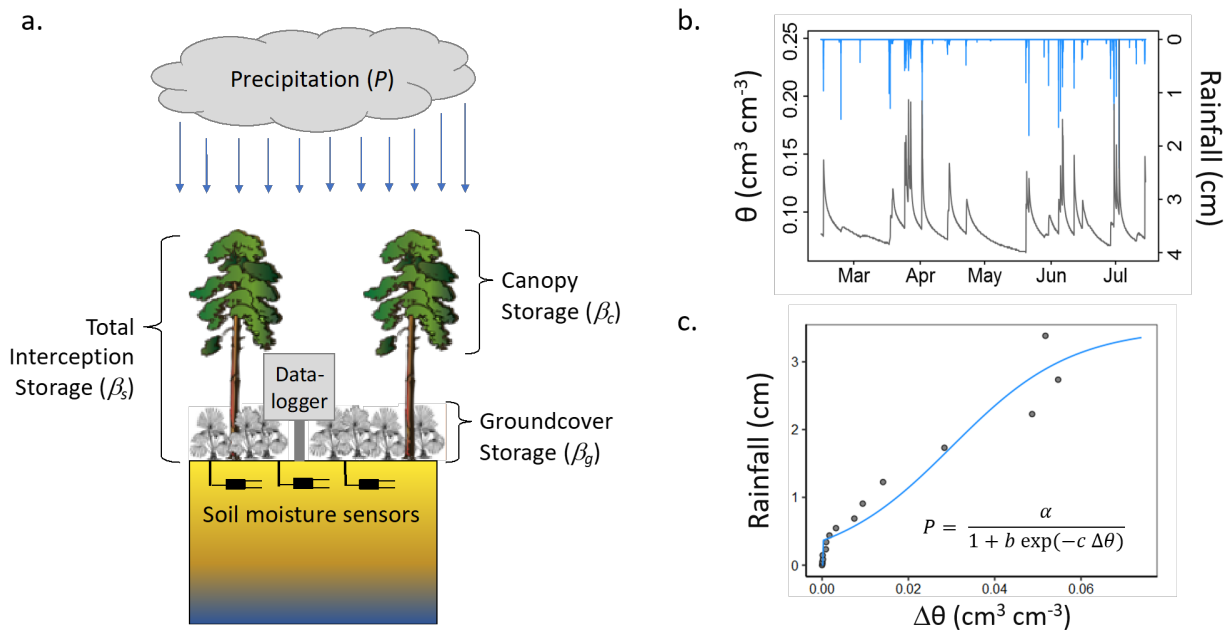

561

562 Figure 1. (a) Schematic illustration of experimental setup and interception water storages, where
563 total interception storage (β_s) is the sum of canopy storage (β_c) and groundcover (understory and
564 litter) storage (β_g). (b) Example time series of rainfall (blue lines) and corresponding near-
565 surface soil moisture content (θ, black line; observed at 15 cm in this study). (c) Resultant
566 relationship between rainfall and change in soil moisture $\Delta\theta$ during rainfall, along with fitted
567 model to extract the y-intercept (i.e., P_s).

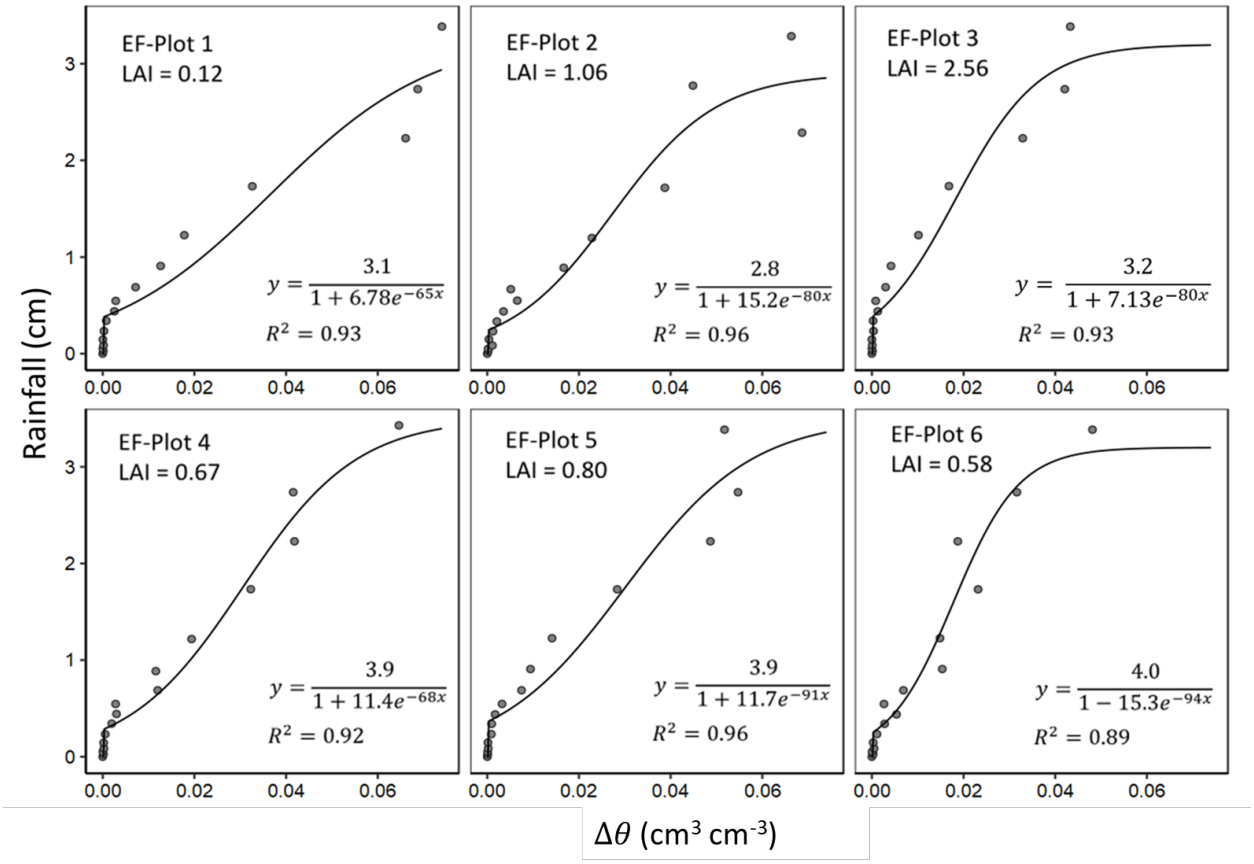

568

569 Figure 2: Binned rainfall depths vs change in soil moisture content ($\Delta\theta$) for six plots at one of the

570 study sites used in the study (Econfina; EF). The y-intercept of the fitted relationships were used

571 to derive P_s in Eq. 2. Note different y-axis scale for EF-Plot 3.

572

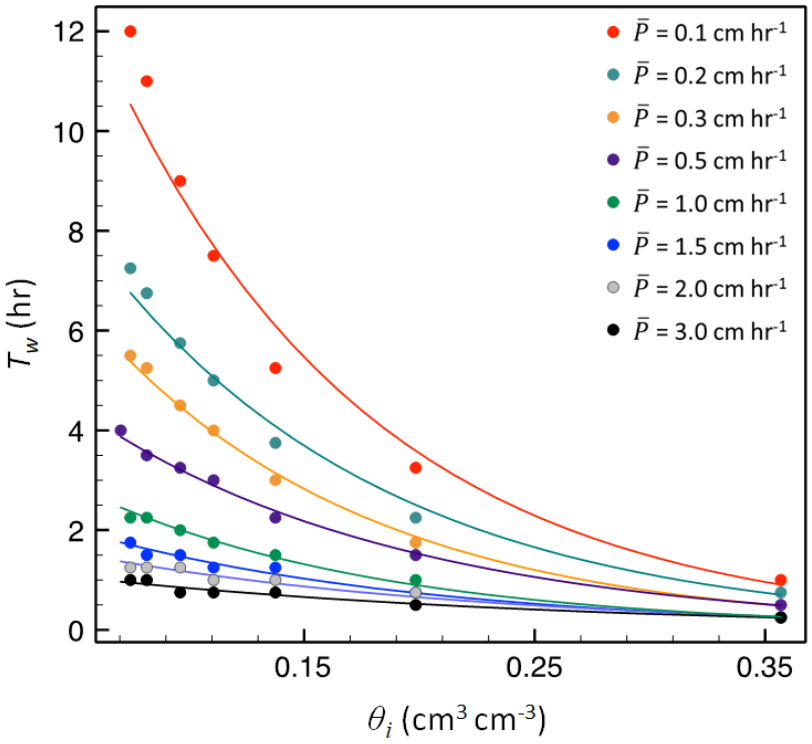

573

574 Figure 3: Initial soil moisture content (θ_i) versus time of wetting front arrival (T_w) at 15 cm depth

575 for a loamy sand soil. Dots are simulated results from HYDUS-1D simulation, and lines are the

576 exponential model given in Eq. 8, fitted for each rainfall rate, $\bar{P}$.

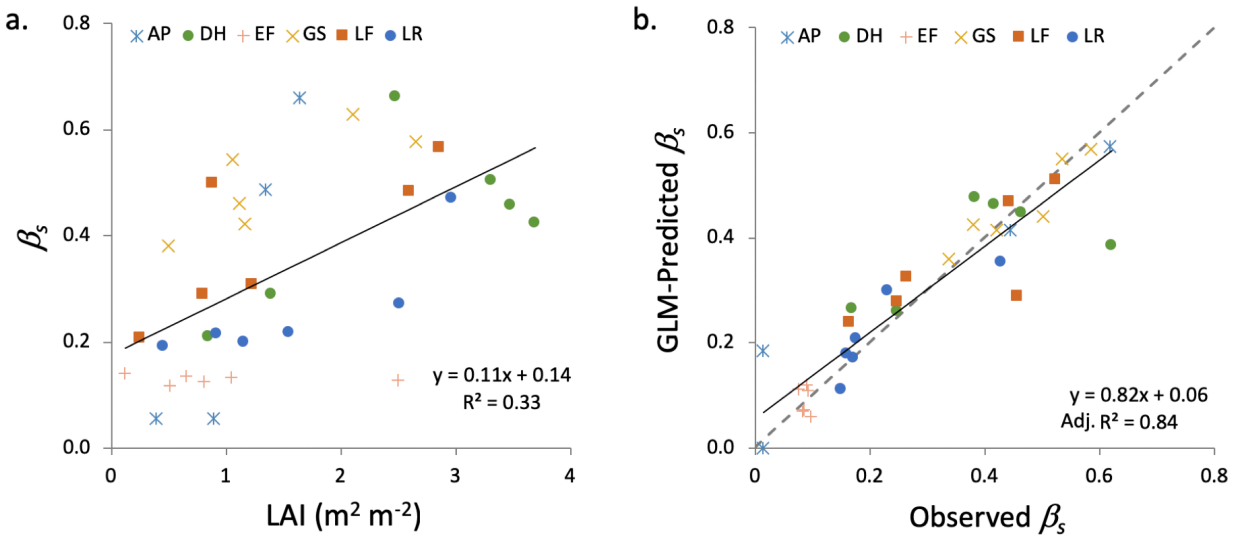

577

578 Figure 4. (a) Interception storage capacity (β_s) versus leaf area index (LAI) for all sites and plots.

579 (b) Modeled versus observed β_s using the best GLM, which included % groundcover vegetation

580 and an interaction term between site and LAI. The dashed line is the 1:1 line.

581

582

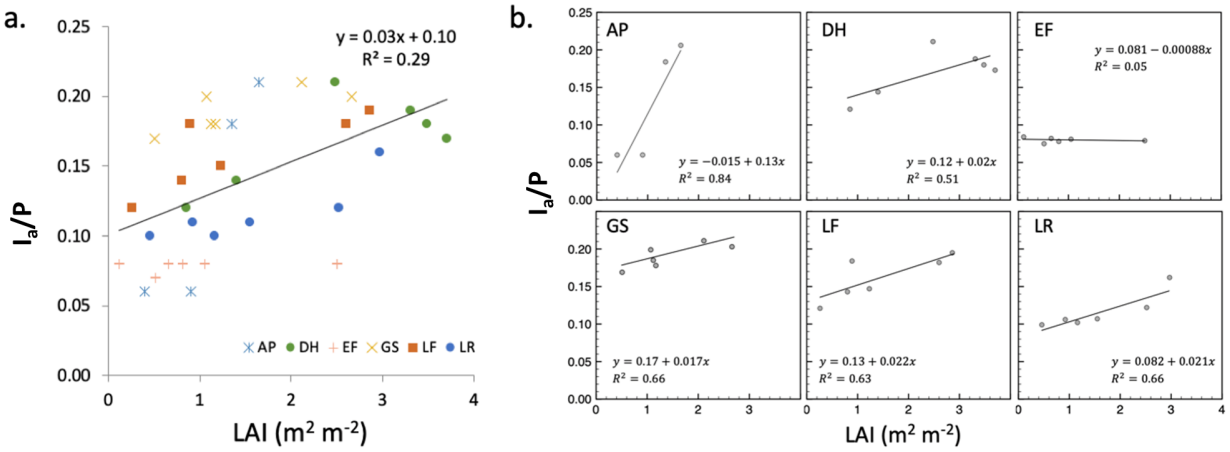

583
584

585 Figure 5. (a) Annual proportion of rainfall that is intercepted (I_a/P) intercepted versus LAI for all

586 sites and plots. (b) Site-specific I_a/P versus LAI relationships. The relationship is generally

587 strong except for the EF site, where the overall storage capacity is small across all values of LAI.

588

589 Table 1. Summary of storage capacity (β_s) and annual interception losses (I_a) for all sites and
590 plots, along with plot characteristics (mean annual precipitation, P; leaf area index, LAI; percent
591 groundcover, %GC; and species). Note that the AP site only had four plots with the data required
592 for the analysis.

Site	Plot	LAI	%GC	Species	β_s (cm)	R^2 ($\Delta\theta$-P)	P (cm)	I_a/P
AP	2	1.65	47.6	SF Slash	0.620	0.31	145.0	0.206
AP	3	0.90	62.8	SF Slash	0.014	0.78	145.0	0.06
AP	4	1.35	49.1	SF Slash	0.445	0.67	145.0	0.184
AP	6	0.40	73.4	Longleaf	0.014	0.57	145.0	0.06
DH	1	0.85	86.2	Loblolly	0.170	0.90	131.5	0.121
DH	2	2.48	51.2	Slash	0.621	0.68	131.5	0.211
DH	3	1.40	39.2	Slash	0.249	0.49	131.5	0.144
DH	4	3.31	35.8	Slash	0.464	0.71	131.5	0.188
DH	5	3.70	27.1	Loblolly	0.383	0.69	131.5	0.173
DH	6	3.48	32.9	Slash	0.418	0.40	131.5	0.18
EF	1	0.12	13.6	Clearcut	0.099	0.93	153.8	0.084
EF	2	1.05	56.9	Slash	0.092	0.96	153.8	0.081
EF	3	2.50	11.8	Sand	0.086	0.93	153.8	0.079
EF	4	0.66	50.9	Slash	0.094	0.92	153.8	0.082
EF	5	0.81	17.9	Sand	0.085	0.96	153.8	0.078
EF	6	0.52	52.0	Longleaf	0.076	0.89	153.8	0.075
GS	1	1.07	67.9	Clearcut	0.502	0.84	132.4	0.199
GS	2	2.66	7.9	Slash	0.535	0.88	132.4	0.203
GS	3	2.11	71.5	Slash	0.587	0.82	132.4	0.211
GS	4	1.12	42.4	Slash	0.421	0.90	132.4	0.185
GS	5	1.17	45.6	Slash	0.382	0.76	132.4	0.178
GS	6	0.51	55.2	Longleaf	0.339	0.78	132.4	0.169
LF	1	0.26	43.5	None	0.166	0.85	136.3	0.121
LF	2	2.86	23.1	Slash	0.525	0.64	136.3	0.195
LF	3	1.23	24.9	Slash	0.266	0.72	136.3	0.147
LF	4	0.80	25.7	Slash	0.248	0.64	136.3	0.143
LF	5	2.60	12.3	Slash	0.443	0.63	136.3	0.182
LF	6	0.89	25.9	Longleaf	0.458	0.69	136.3	0.184
LR	1	0.46	34.0	Clearcut	0.151	0.96	144.5	0.099
LR	2	2.97	38.1	Slash	0.429	0.84	144.5	0.162
LR	3	0.92	47.0	Slash	0.173	0.95	144.5	0.106
LR	4	2.52	26.7	Slash	0.232	0.92	144.5	0.122
LR	5	1.55	28.1	Slash	0.177	0.96	144.5	0.107
LR	6	1.16	35.5	Longleaf	0.160	0.96	144.5	0.102

593

Table 2. Summary of generalized linear model (GLM) results for interception storage capacity (β_s). LAI is leaf area index, GC is groundcover, and WT is water table (shallow vs. deep). The best model (by AIC) is shown in bold.

Model #	Variable(s)	AIC	R^2
1	LAI	378.1	0.32
2	LAI + site	318.5	0.66
3	LAI * site	255.9	0.83
4	**LAI * site + GC**	**253.1**	**0.84**
5	LAI + WT	338.3	0.55
6	LAI * WT	339.8	0.55
7	LAI * WT + GC	341.8	0.55
8	LAI + WT + GC	340.3	0.55